Comptes Rendus
Chimie
Supplementary material to the article available at:
https://doi.org/10.5802/crchim.227

Supplementary material: Influence of sulfate-reducing bacteria on the biocorrosion of mild steel coated with hybrid polyetherimide-ZnO or CuO bilayer composites

Document complémentaire : Influence des bactéries sulfato-réductrices sur la biocorrosion de l'acier doux revêtu de composites bicouches hybrides polyétherimide-ZnO ou CuO

Emna Rahali[a, b], Leila El-Bassi[*, a], Latifa Bousselmi[a], Marta M. Alves[c], Maria de Fátima Montemor[c] and Hanene Akrout[a]

[a] Laboratory for Wastewater and Environment, Water Researches and Technologies Center (CERTE), Technopark of Borj Cedria, PB 273, Soliman 8020, Tunisia

[b] National Institute of Applied Science and Technology (INSAT), Carthage University, Tunis, Tunisia

[c] Centro de Química Estrutural, Institute of Molecular Sciences, Departamento de Engenharia Química, Instituto Superior Técnico, Universidade de Lisboa, Av. Rovisco Pais 1049-001, Lisboa, Portugal

E-mails: rahali93@hotmail.com (E. Rahali), l.elbassi@gmail.com (L. El-Bassi), latifa.bousselmi.certe@gmail.com (L. Bousselmi), marta4alves@gmail.com (M. M. Alves), mfmontemor@tecnico.ulisboa.pt (M. F. Montemor), Hanene.akrout@yahoo.com (H. Akrout)

According to our previous research [1], the morphological analysis proved that thesecond layered coatings have homogenously distributed holes resulting from solvent evaporation (Figure S1). Different morphologies were observed within the PEI coatings. The PEI alone showed larger holes than the PEI-metal oxides. This may somehow result from the physical interaction of the oxide particles with the solvent during the evaporation process [1].

Detailed surface analysis was made further to analyze the oxide particles distribution within the com-

* Corresponding author.

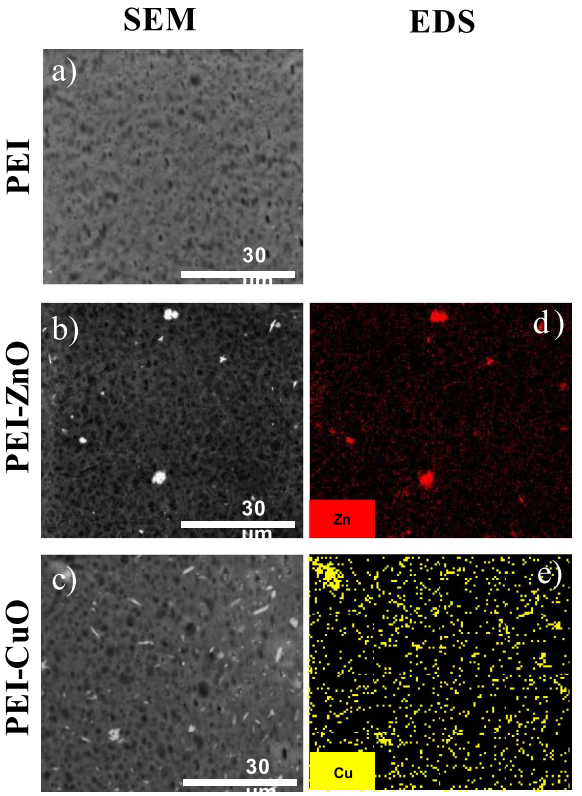

Supplementary Figure S1. Physicochemical characterization of the bilayer composite coatings; top-view SEM images of (a) PEI, (b) PEI-ZnO and (c) PEI-CuO, and corresponding EDS maps of (d) Zn and (e) Cu.

Supplementary Table S1. Composition of artificial wastewaters

Composition (mg/l)	NaCl	Na_2SO_4	$NaNO_2$	Na_3PO_4
ATWW	742.059	265.880	148.48	2.3

posite coatings. As depicted in Figure S1b–e, the bright structures visible on the surface (Figure S1b,c), coincident with the EDS map distribution for Zn (Figure S1d) and Cu (Figure S1e), depict ZnO and CuO on the coatings, respectively.

Representative Nyquist and Bode plots (Figure S2) were obtained for bare MS immersed in ATWW with and without bacteria. After 7 days of immersion, the EIS result for bare MS in the abiotic system showed two-time constants. The time constant at high frequencies can be assigned to the formation of a porous corrosion layer (Figure S3e) [1]. The second time constant, at lower frequencies, can be related to the faradic responses being at the interface metal/electrolyte [2]. To scrutinize the EIS data, the electrochemical parameters were estimated by fitting the experimental data using the equivalent electric circuit (EEC) depicted in Figure S2c [3], where R_s is the electrolyte resistance, the R_{film} and Q_{film} are respectively the resistance and the constant phase element of the outer corrosion layer, R_{ct} and CPE_{dl}, represent the faradic resistance and the double-layer constant phase element, respectively. The fitting data are illustrated in Table S2, and the validity of the data was confirmed by chi-square values (χ^2) falling in the ranges of 10^{-4} or below.

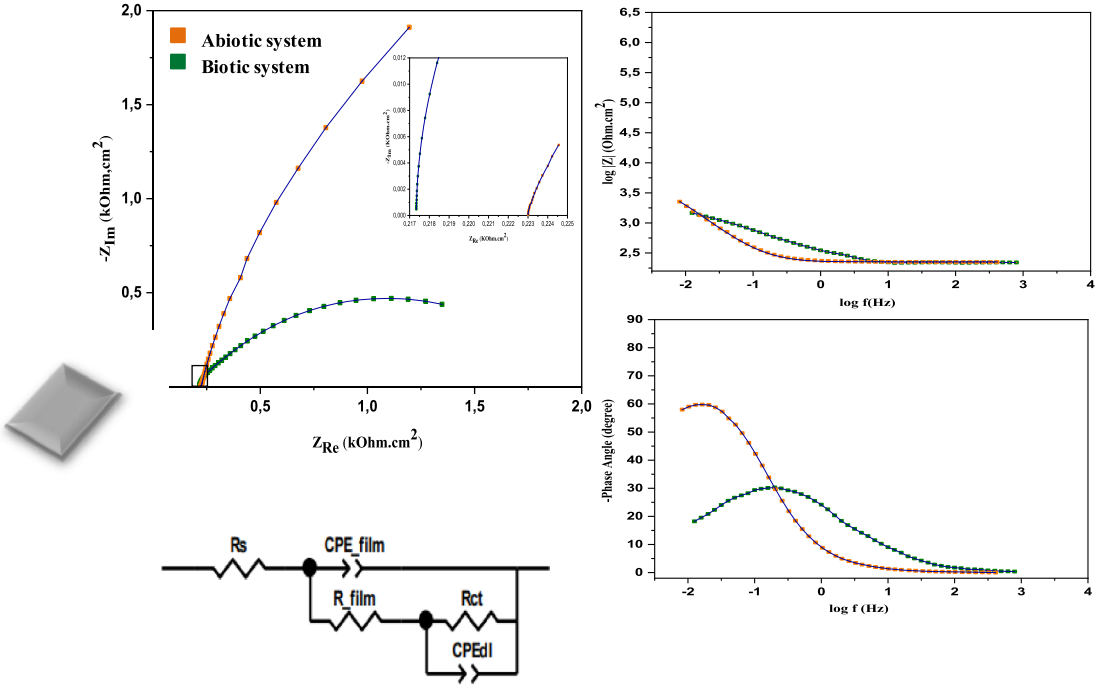

Supplementary Figure S2. Nyquist and Bode plots of bare mild steel immersed in abiotic system (ATWW) and biotic system (ATWW + *Desulfovibrio*), and the equivalent circuit used to fit the EIS data.

Supplementary Table S2. Evolution of impedance parameters of bare mild steel immersed in Abiotic and biotic system

Medium Parameter	Abiotic system (ATWW)	Biotic system (ATWW + *Desulfovibrio sp.*)
R_s ($\Omega\cdot cm^2$)	210.4	223.4
R_f ($\Omega\cdot cm^2$)	820	350
Q_f ($\Omega^{-1}\cdot cm^2\cdot s^n$)	9×10^{-4}	5×10^{-3}
n_1	0.8	0.86
R_{ct} ($\Omega\cdot cm^2$)	1918	1200
Q_{dl} ($\Omega^{-1}\cdot cm^2\cdot s^n$)	2.2×10^{-5}	4×10^{-3}
n_2	0.6	0.83
$\chi 2$	5×10^{-4}	2.5×10^{-5}

In the presence of *Desulfovibrio* sp, during exponential phase (4–7 days), bacteria colonized the steel surface (Figure S1A-a), with an anticipated accumulation of their metabolic products [4]. Plots show that the total impedance (Figure S3a) values at lower frequencies showed a slight decrease compared to diagrams without bacteria (Figure S3b).

The data in Table S2 shows reduction in the faradic resistance, R_{ct}. This decrease is mainly due to SRB bio-catalytic activities. In fact, SRB species can enhance the redox activity of the medium and accelerate iron dissolution [5]. The aggressive factors of the biofilm and the active metabolisms of the sessile bacteria such as EPS assembly (Figure S1C) and the reported acetate production alter the electrochemical process, subsequently changing the pH by the resulting hydrogen sulfide (H_2S) [5]. Werner *et al.* [6] reported that SRB can primarily create a biofilm with a crevice-like geometry on the steel surface, and H_2S production that can increase the corrosion conditions on the metal surface [6]. H_2S reacts with Fe ions to form iron sulphide (Figure S3a) [6]. The presence

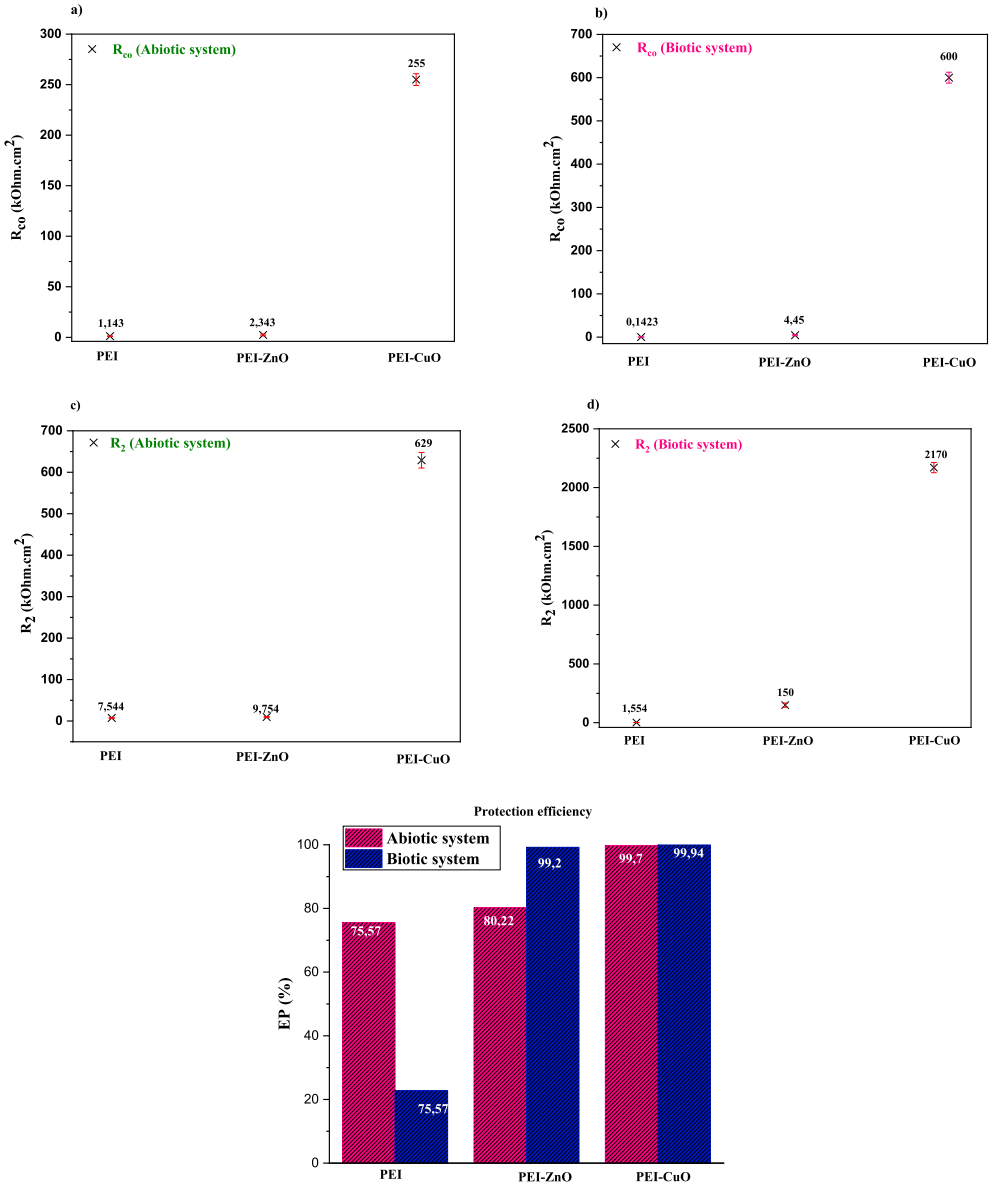

Supplementary Figure S3. Evolution of R_f and R_{ct} in abiotic system (a,c) and (b,d) biotic system, (e) protection efficiency.

of FeS and iron oxides accelerate the anodic dissolution of steel [7,8].

Therefore, it is relevant to find innovative solutions to effectively mitigate the corrosive effects of SRB biofilms. This can be achieved by protecting MS with polymeric agents, as PEI, or by the additional incorporation of antimicrobial agents as ZnO or CuO [9,10].

Figure S3 shows the increase in the corrosion protection efficiency (PE) determined by the following equation [11] in the abiotic and biotic systems:

$$\text{PE}(\%) = \frac{R_2 - R_{\text{ct}}}{R_{\text{ct}}} \times 100 \qquad (3)$$

where R_2 is the faradic resistance of the coated steel and R_{ct} is the faradic resistance of bare mild steel.

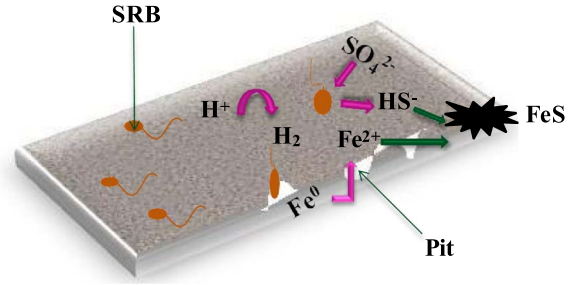

Supplementary Figure S4. Experimental design used to illustrate the SRB corrosion process of mild steel.

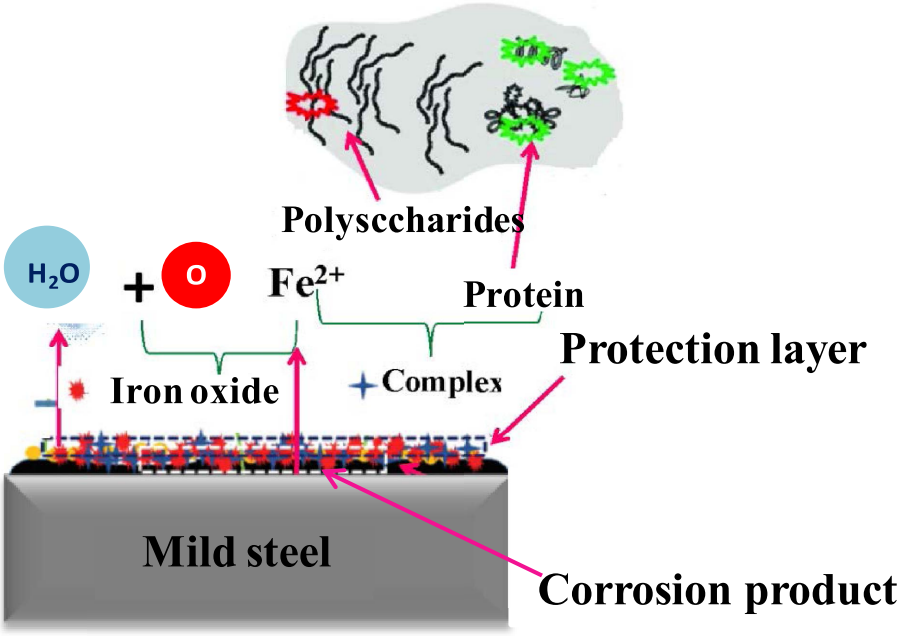

Supplementary Figure S5. Mechanism of (Chelates-corrosion products) protective layer.

References

[1] E. Rahali, M. M. Alves, L. El-Bassi, L. Bousselmi, M. F. Montemor, H. Akrout, *Prog. Org. Coat.*, 2022, **163**, article no. 106602.

[2] M. Behzadnasab, S. M. Mirabedini, K. Kabiri, S. Jamali, *Corros. Sci.*, 2011, **53**, 89-98.

[3] Y. Peng, A. E. Hughes, G. B. Deacon, P. C. Junk, B. R. W. Hinton, M. Forsyth, J. I. Mardel, A. E. Somers, *Corros. Sci.*, 2018, **145**, 199-211.

[4] I. Ziadi, M. M. Alves, M. Taryba, L. El-Bassi, L. Bousselmi, M. F. Montemor, H. Akrout, *Bioelectrochemistry*, 2020, **132**, article no. 107413.

[5] F. M. Al Abbas, R. Bhola, J. R. Spear, D. L. Olson, B. Mishra, *Int. J. Electrochem. Sci.*, 2013, **8**, 859-871.

[6] S. E. Werner, C. A. Johnson, N. J. Laycock, P. T. Wilson, B. J. Webster, *Corros. Sci.*, 1998, **40**, 465-480.

[7] F. Batmanghelich, L. Li, Y. Seo, *Corros. Sci.*, 2017, **121**, 94-104.

[8] C. S. Frings, T. W. Fendley, R. T. Dunn, C. A. Queen, *Clin. Chem.*, 1972, **18**, 673-674.

[9] K. Alasvand Zarasvand, V. R. Rai, *3 Biotech*, 2016, **6**, 1-7.

[10] W. Artifon, S. M. Pasini, A. Valério, S. Y. G. González, S. M. de Arruda Guelli Ulson de Souza, A. A. U. de Souza, *Mater. Sci. Eng. C*, 2019, **103**, article no. 109859.

[11] R. Rajkumar, C. Vedhi, *Anti-Corros. Method. M.*, 2020, **67**, 305-312.